Designed Regular Tetragon-Shaped RNA–Protein Complexes with Ribosomal Protein L1 for Bionanotechnology and Synthetic Biology

Hirohisa Ohno and Tan Inoue*

Laboratory of Gene Biodynamics, Graduate School of Biostudies, Kyoto University, Kitashirakawa Oiwake-cho, Sakyo-ku, Kyoto 606-8502, Japan

ABSTRACT RNA nanotechnology has been established by employing the molecular architecture of RNA structural motifs. Here, we report two designed RNA–protein complexes (RNPs) composed of ribosomal protein L1 (RPL1) and its RNA-binding motif that are square-shaped nano-objects. The formation and the shape of the objects were confirmed by gel electrophoresis analysis and atomic force microscopy, respectively. Any protein can be attached to the RNA *via* a fusion protein with RPL1, indicating that it can be used as a scaffold for loading a variety of functional proteins or for building higher-order structures. In summary, the RNP object will serve as a useful tool in the fields of bionanotechnology and synthetic biology. Moreover, the RNP interaction enhances the RNA stability against nucleases, rendering these complexes stable in cells.

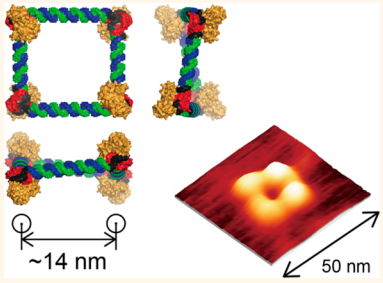

KEYWORDS: RNA nanotechnology · RNA–protein interacting module · RNP nanostructures · ribosomal protein L1 · bionanotechnology · synthetic biology

Nucleic acids have been convenient materials in the field of nanotechnology due to their ability to self-assemble and self-organize.[1,2] In addition to base-complementarity similar to that of DNA, RNA with unique higher-order structures and biological functions has been utilized as another class of these materials. Naturally occurring RNA molecules often show highly complicated three-dimensional structures and consist of various structural modules, and they can be used as building blocks for designing and constructing artificial nano-objects.[3] Thus far, a variety of RNA nano-objects have been reported[4−13] that are useful in the fields of nanomedicine, nanotechnology, and synthetic biology.[14,15]

Many RNAs play biological roles as molecular complexes with proteins. Highly evolved RNA–protein complexes, such as the ribosome and spliceosome, have extremely complicated structures with sophisticated functions. We have shown that a naturally occurring RNA–protein interacting module (RNP module) in the complexes can be used to design and build a new artificial RNP. In our previous study, we demonstrated the design and construction of triangular nano-objects created with the box C/D RNA–L7Ae protein interacting module found in a ribosome.[16] The RNP objects were used as scaffolds for functional RNAs and proteins.[17] Moreover, they are able to quantitatively regulate the signal transduction from a human cell surface receptor depending on the distance between the attached receptor-binding proteins.[18]

A variety of modules are needed to design and construct more useful molecules with elaborate structures that enable sophisticated functions. However, only a few naturally occurring RNP modules have been employed. Thus, we are exploring a variety of RNP modules for further development.

Here, we used an RNP module consisting of the ribosomal protein RPL1 (from a thermophilic archaea, *Methanocaldococcus jannaschii*) and the corresponding RNA motif (Figure 1a). RPL1 binds to a specific

* Address correspondence to tan@kuchem.kyoto-u.ac.jp.

Received for review December 6, 2014 and accepted May 1, 2015.

Published online May 01, 2015
10.1021/nn5069622

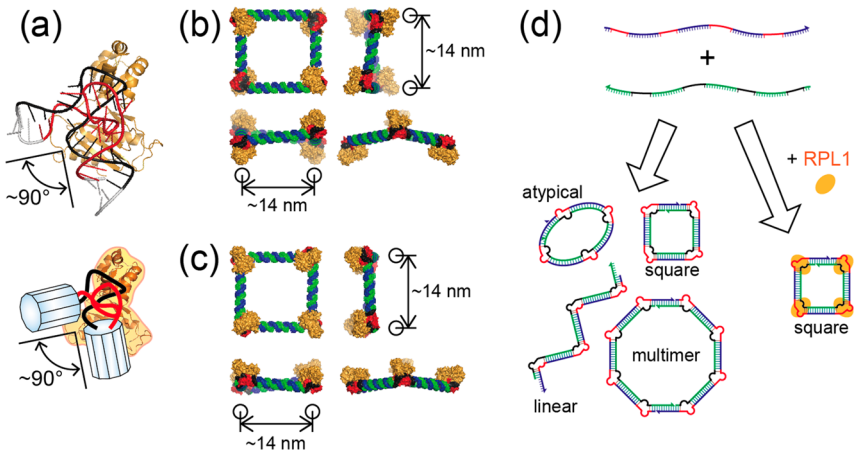

Figure 1. Design of square-shaped RNP. (a) Three-dimensional structure (top) and its schematic representation (bottom) of the RPL1−rRNA motif. RPL1 (orange)-bound RNA is kinked and fixed at ~90°. (b,c) Three-dimensional models of square-shaped RNPs. Both squares consist of two RNA strands (blue and green) and four RPL1 proteins (orange). (d) Schematic representation of the regulation of structural changes by RPL1.

region in 23S rRNA, and the domain composed of the complex is implicated in the deacylated tRNA release from the ribosome during translation.[19,20] RPL1 also binds to a specific site on its own mRNA, thereby downregulating its protein expression.[21−23] These two RPL1-binding RNA motifs share a common sequence and a similar three-dimensional structure (Supporting Information Figure S1a). In the RNP complexes, both RNAs are fixed at a right angle.[24,25] Thus, both RNP complexes can be used as an equivalent building block for constructing new RNP nano-objects, although their binding affinities differ considerably.[26] We confirmed that the rRNA motif possesses superior binding affinity and specificity compared to the mRNA motif (Supporting Information Figure S1b). Therefore, we used the RPL1−rRNA motif as the building block.

RESULTS AND DISCUSSION

We designed a regular tetragon-shaped RNP nanostructure by using the right-angle RNP motif. Four RNP motifs were connected with four double-stranded RNAs (dsRNAs) to build a planar square structure and minimize distortion. Two classes of regular tetragon molecules were designed because two directions are available for inserting the RPL1−rRNA motifs. One class is a flip-flop type in which the two RPL1 proteins located on the diagonally opposite corners protrude from the same face, while the other two proteins located on the other corners protrude from the other face (Figure 1b and Supporting Information Figure S2a). The other class is a unilateral type in which all of the RPL1 proteins protrude from the same face of the square plane (Figure 1c and Supporting Information Figure S2b). These constructs consist of two RNAs (RNA1 (blue) and RNA2 (green) in Figure 1 and Supporting Information Figure S2) and four RPL1s.

RPL1 is likely to induce a structural alteration to its RNA counterpart, as in the case of the L7Ae protein and its RNA counterpart. The bound RPL1s that fix the corners to a right angle should induce a square shape to the RNA that is otherwise flexible (Figure 1d).

The electrophoretic mobility shift assay (EMSA) was performed to examine the interaction between the RNA and the RPL1 in the complex. Retardation of the RNA band was observed for both flip-flop and unilateral complexes upon increasing the concentration of RPL1, indicating that the RNA interacted with the protein (Figure 2). The band shift seemed to proceed with only one instead of four gradual steps under these conditions, indicating that the RNA and the four RPL1s interacted cooperatively. For instance, one bound RPL1 might have stabilized the whole RNA structure to promote facile interactions with the additional RPL1. Meanwhile, smeary upper bands appeared in the lanes with highly concentrated RPL1 for both cases. This is presumably due to nonspecific interaction of excess RPL1 protein with the RNA that is consistent with the result in Supporting Information Figure S1b. Under these conditions, 50 nM RNA with 200 nM RPL1-binding motifs was completely gel-shifted in the presence of 600 nM RPL1 for both constructs. Therefore, the same ratio was adopted in subsequent experiments.

The hydraulic size of the RNP was analyzed by dynamic light scattering. In both constructs, the RNA with the RPL1 protein was larger than that without the protein (Supporting Information Figure S3), implying the formation of the RNP complex. The formation of the RNP complexes with the four proteins was confirmed by using the atomic force microscope (AFM), as we discuss later.

To evaluate the structures, AFM imaging was performed on the RNA alone and with RPL1 under air conditions. In the case of the RNA alone, most of the objects were rod-shaped, although some linear and large circular objects were observed for both constructs

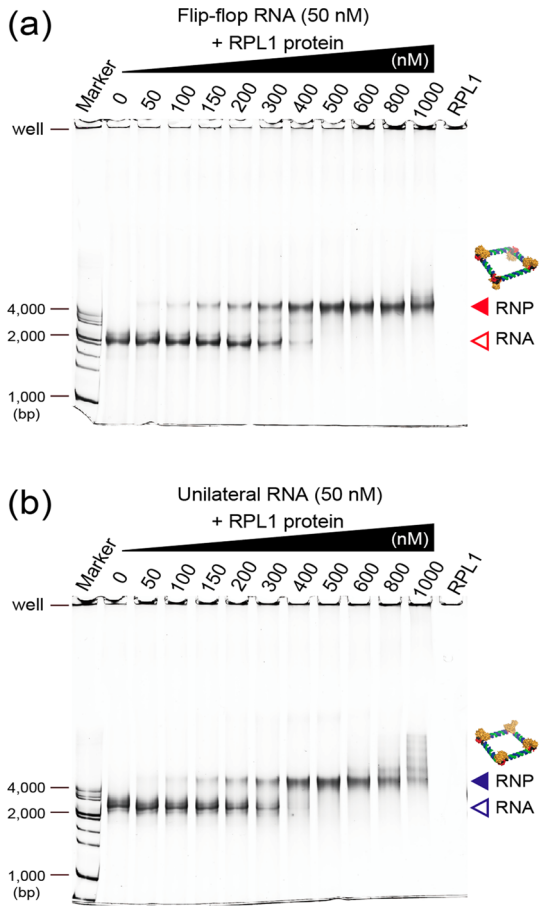

Figure 2. Electrophoretic mobility shift assay. Interactions between designed RNA and RPL1 proteins were confirmed by EMSA in both flip-flop (a) and unilateral (b) squares. The delayed mobility of the band by increasing RPL1 protein indicates the RNP complex formation. Marker, DNA ladder marker; RPL, RPL1 (1000 nM).

(Supporting Information Figure S4). The structural heterogeneity likely reflects the flexibility of the RNAs. In contrast, square-shaped objects were observed, and linear and large circular-shaped objects were barely visible in the presence of either RNA with RPL1, indicating that the RPL1 protein induced the structural alteration (Figure 3a,b).

The sizes of the RNP squares were measured by the lengths between the midpoints of the opposite sides. The average size in the flip-flop and unilateral RNP was 12.9 ± 1.3 and 12.8 ± 1.4 nm, respectively (Figure 3c,d). The values corresponded well to their 3D models (Figure 1b,c). The average height at the side was 1.48 ± 0.42 and 1.47 ± 0.43 nm for the flip-flop and unilateral RNP, respectively (Supporting Information Figure S5). These heights are consistent with the ~1.5 nm reported height of other square-shaped RNA particles.[5] In addition, the heights at the corners were 1.83 ± 0.37 and 1.72 ± 0.41 nm for the flip-flop and unilateral RNP, respectively, suggesting that the small increase was due to the bound RPL1s (Supporting Information Figure S5).

The rhombus-shaped quadrilaterals were more often observed in the flip-flop than in the unilateral type. The ratio of the diagonal lengths and the ratio of the widths were measured (Supporting Information Figure S6). The rhombus-shaped particles (36%) were more abundant than the squares (30%) in the flip-flop type, whereas the squares (36%) were more frequently observed than the rhombus-shaped ones (26%) in the unilateral type. This finding could be attributed to the flatness of the structure. Presumably, the flip-flop square has to be distorted on the planar mica surface because it is less flat than the unilateral square (Figure 1b,c). The 3D models support the observed difference.

High-resolution analyses were attempted with high-speed AFM under liquid conditions. The complex with four RPL1s was not identified for the flip-flop type. Most of the complexes included only one or two RPL1s (Supporting Information Figure S7a). This is presumably due to their three-dimensional structure because all of the possible complexes (four, three, two, and one RPL1) were visible on the RNA in the unilateral square (Supporting Information Figure S7b). Their bent structure is likely unsuitable for interaction with the planar mica surface compared to the unilateral type. The bound proteins presumably protrude and decrease the flatness (Figure 1a) to weaken the interaction.

The reason that fewer fully loaded complexes were observed by high-speed AFM could be attributed to the detachment of the proteins from the RNA during the experimental manipulations (*e.g.*, dilution, fixation to the mica surface, and tapping by a cantilever). In fact, the dissociation of the proteins from RNA was observed during the imaging, indicating that the actual yield of the complete complex was higher than that observed in the AFM data.

The RNP squares can be used as a carrier for functional RNAs, such as siRNA or aptamers. As an example, the RNA aptamer was introduced into the unilateral square RNPs (Supporting Information Figure S8a–c). The malachite green (MG) aptamer was introduced to the RNA stems to increase the fluorescence of MG on the RNA when the aptamer specifically binds to MG.[12,27–29] As expected, the RNP square containing the MG aptamer resulted in enhanced fluorescence in the presence of MG (Supporting Information Figure S8d). The interaction between the RNA and RPL1 had no influence on the binding ability of the aptamer, demonstrating that the RNP can be functionalized with a functional RNA.

The chemical and biochemical instabilities of RNA have been a problem for its applications in cells. Chemical modifications, such as 2′-fluororibose, can confer resistance to RNases.[12] However, these modifications sometimes have adverse impacts on the inherent structures and functions of the RNA. Interestingly, it was shown that RNPs are more tolerant to RNases than unmodified RNA.[17]

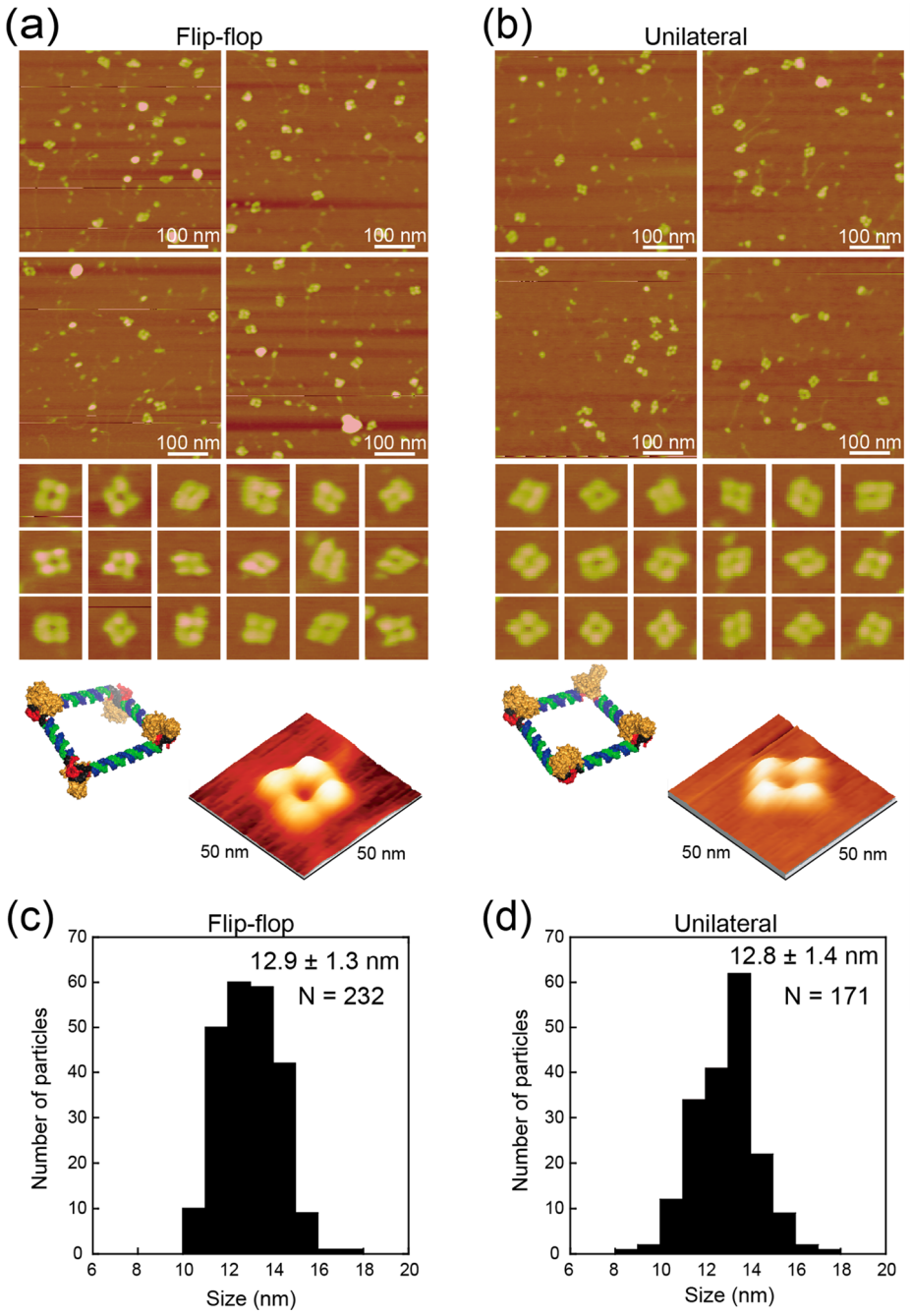

Figure 3. AFM imaging of the RNP complex. AFM images (500 × 500 nm, top) and magnifications of square-like particles (50 × 50 nm, middle) for flip-flop (a) and unilateral (b) squares. Three-dimensional surface images are also shown (bottom). (c,d) Size distribution of square-like particles; *N* = 232 and 171, respectively.

To assess whether RPL1 has a protective effect in the RNP, the flip-flop and unilateral RNAs were incubated at 37 °C in 20% fetal bovine serum (FBS)-containing buffer with or without RPL1 (Supporting Information Figure S9). For both constructs, more than 50% of the RNAs remained intact after 24 h in the presence of RPL1, while the RNAs by themselves were completely degraded after 8 h of incubation (Figure 4). This protection is presumably due to steric hindrance by the RPL1 that protects the RNA from RNases. Thus, the RNP constructs are likely more stable than the RNA by itself in the presence of RNases, indicating that they are useful for applications in cells. Further improvement seems possible by introducing additional modifications to the marginal regions.

We performed the melting curve analysis with SYBR Green by employing a real-time polymerase chain reaction (PCR) device (Supporting Information Figure S10). The temperature-dependent decrease of the fluorescence showed very similar tendency either in the presence or in the absence of RPL1

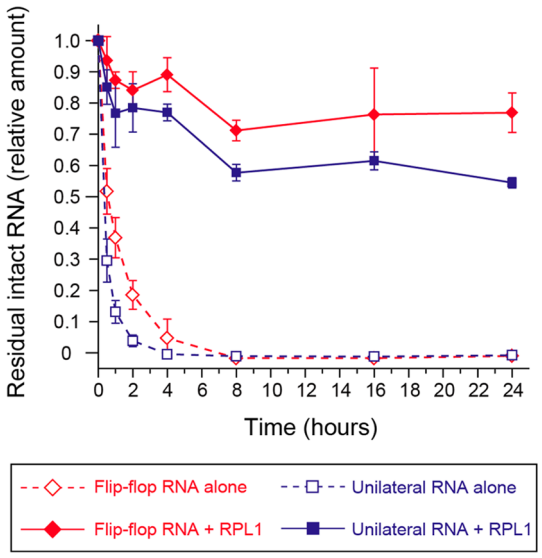

Figure 4. RNA protection by RNP complex formation. The square RNAs with/without RPL1 protein were incubated in 20% FBS-containing buffer (see also Supporting Information Figure S8). In both flip-flop (red) and unilateral (blue) squares, the RNP complex (solid box and solid line) showed increased stability compared to RNA alone (open box and dashed line).

(Supporting Information Figure S10), implying that RPL1 does not influence the RNA thermostability.

One advantage of using RNPs in biological applications is that the RNA and protein can be synthesized in cells by introducing their corresponding genes, indicating that the RNP nanostructures can also be constructed in cells. To implement the in-cell construction, it is necessary for the RNP to fold accurately under isothermal conditions[28,30] instead of the denaturing-to-renaturing conditions employed in this study. Thus, we attempted to determine whether the square RNP could be formed under isothermal conditions. The RNAs with or without the proteins were mixed and incubated at 37 °C *in vitro* (Supporting Information Figure S11). The results showed that the RNAs were hybridized effectively, but the yield was lower than that with the denaturing-to-renaturing conditions. The efficiency can be improved by optimizing the sequences at the dsRNA regions or appropriately controlling the quantity and time of expression in the target cells. The RNP production in cells could be beneficial in future applications, such as the design of scaffolds to collect desired proteins to exert artificial cell functions.[31,32] As described, the RNP complex including RPL1 has improved resistance against RNases. This development will be advantageous for future applications, including drug delivery systems.

CONCLUSION

In conclusion, we have demonstrated that the RPL1−rRNA motif can be used as a building block with a right-angle shape for constructing two types of square-shaped RNP structures. The RPL1−rRNA motif can regulate the RNA structure in the presence or absence of RPL1, in contrast to the previously reported RNA that forms roughly quadrangular structures by itself.[5]

The RNPs will be useful as carriers of functional RNAs, such as siRNA and aptamers.[7,9,12,13,17,29] Furthermore, any protein can be attached to the RPL1 to form the RNP containing the desired fusion proteins. The resulting fusion proteins will be located toward the center of the square due to the positions of the termini in RPL1, unlike triangular RNP, which presents the fusion proteins outward.[16,17] This feature will be useful for specifically assembling a target protein in a desired manner by employing the flip-flop or unilateral RNP. For example, the flip-flop type can be used to assemble multiple cells by attaching a specific cell-binding antibody fused to RPL1, whereas an individual cell can be the target of the unilateral type without inducing cell assembly. Moreover, the square-shaped RNP could serve as a basic unit for building higher-order structures. For example, a large filament-like structure might be formed when a dimeric RPL1 and the flip-flop type RNA are used.

Recently, protein nanostructures have been reported.[33−35] These protein nanotechnologies can be easily and directly combined with the RNA nanotechnology through the RNP module and RNP nanostructures. Many naturally occurring RNP structural motifs are available other than RPL1 and L7Ae.[36] Thus, further development of this class of RNP bionanotechnology is possible and promising.

METHODS

Design of Square RNPs. Our RPL1 construct was from a thermophilic archaeon, *M. jannaschii* (construct referred to as MjaL1). The crystal structure of its complex with an mRNA motif has been determined (PDB ID: 1U63),[25] but no structure in complex with an rRNA motif exists. A structure of another complex with rRNA was reported using RPL1 from a thermoacidophilic archaeon, *Sulfolobus acidocaldarius* (PDB ID: 1MZP; construct referred to as SacL1).[24] To use the 3D data of the SacL1−rRNA complex instead of MjaL1, we compared their 3D structures. Both protein structures were similar, and the amino acid residues interacting with RNA were well conserved. The protein-interacting surfaces on the RNAs also shared similar structures.[25] Therefore, we expected that MjaL1 could interact with an rRNA motif and fix the RNA to a 90° angle, as with SacL1. The binding between MjaL1 and the rRNA motif was confirmed (Supporting Information Figure S1b). Accordingly, we applied the 3D data of the SacL1−rRNA complex (ID: 1MZP) for computational design and used MjaL1 for the actual experiments. The design of square RNPs was performed using the molecular modeling software Discovery Studio (Accelrys). Four RPL1-binding rRNA motifs were connected with four linear dsRNAs to build the square-like structure. The lengths of the dsRNAs were adjusted to form the planar structure and minimize the

distortions on the rRNA motif−dsRNA linking regions, as shown in Supporting Information Figure S2. To avoid the formation of any undesirable structures, suitable sequences were selected from randomly generated sequences and adopted into the side dsRNA regions. All RNA sequences were analyzed by Mfold (http://mfold.rna.albany.edu/) and CentroidFold (http://www.ncrna.org/centroidfold/).

Protein and RNA Synthesis. *RPL1 Protein:.* The RPL1-containing plasmid pMjaL1.4 was kindly provided by Dr. Wolfgang Piendl. The RPL1-encoding region was removed by restriction enzyme digestion and then inserted into the protein expression vector pET-28b(+) with a His-tag for affinity purification. The pET-28b(+)-RPL1 plasmid was transformed into *Escherichia coli* KRX competent cells. Protein expression was induced with rhamnose (final 0.2%), and the culture was incubated overnight at 37 °C. The cells were harvested by centrifugation at 6000 rpm for 20 min at 4 °C and resuspended in sonication buffer (100 mM Tris-HCl, 800 mM NaCl, 100 mM $MgCl_2$, 5 mM 2-mercaptoethanol) at 4 °C. The suspension was sonicated on ice and centrifuged at 6000 rpm for 30 min at 4 °C. After filtration through a 0.22 μm filter (Merck-Millipore), the supernatant was purified with a nickel affinity column HisTrap (GE Healthcare) with imidazole gradient elusion using AKTA explorer 10S (GE Healthcare). The purity of the protein was confirmed by SDS-PAGE. The eluted protein was dialyzed and concentrated using a YM-3 microcon (Merck-Millipore). The protein concentration was determined using the Bio-Rad protein assay (Biorad) and stored in storage buffer (50 mM Tris-HCl, 10 mM $MgCl_2$, 100 mM KCl, 1 mM 2-mercaptoethanol, 50% glycerol, pH 7.5) at −25 °C.

RNAs:. DNA templates for *in vitro* transcription were synthesized by PCR with KOD -Plus- version 2 (Toyobo). Oligo DNAs (shown in the table in the Supporting Information) were purchased from Operon. PCR products were purified with a QIAquick PCR purification kit (Qiagen) and used for *in vitro* transcription using the MEGAshortscript T7 kit (Ambion). Transcribed RNAs were purified by denaturing polyacrylamide gel electrophoresis. The RNA concentration was measured with a NanoDrop spectrophotometer (ThermoScientific).

Electrophoretic Mobility Shift Assay. EMSA samples were prepared containing 50 nM RNA and varying concentrations of RPL1 in 5 μL volumes. For this, 0.25 μL of each RNA (1 μM), 0.9 μL of 5× RPL1-binding buffer (250 mM Tris-HCl, 50 mM $MgCl_2$, 500 mM KCl, pH 7.5), 0.5 μL of 0.1% Nonidet P-40 (Sigma), and 2.6 μL of Milli-Q water were mixed. The mixture was heated at 90 °C for 5 min and then cooled at room temperature for 10 min to fold RNA. Next, 0.5 μL of RPL1 protein (10× concentration) was added to the mixture and incubated at room temperature for 15 min. The mixture combined with 1 μL of gel loading buffer (0.05% dye, 30% glycerol) was loaded into 5% polyacrylamide gel. Electrophoresis was conducted with 0.5× TBE buffer at room temperature. The gel was stained with SYBR Green and observed by an FLA-7000 gel imager (Fuji film).

Atomic Force Microscope Imaging in Air Conditions. RNA or RNP samples were prepared similar to those for EMSA. The sample was diluted 20-fold with 1× RPL1-binding buffer (50 mM Tris-HCl, 10 mM $MgCl_2$, 100 mM KCl, 0.01% Nonidet P-40, pH 7.5). A quantity of 20 μL of the diluted sample solution was applied onto the spermidine-coated mica (treated with 40 μL of 10 mM spermidine for 5 min, diameter: 12 mm) and incubated for 5 min at room temperature for adsorption and fixation. After being washed with 1 mL of Milli-Q water, the mica was dried by a flow of N_2 gas. Then, the mica was observed by NanoScope AFM (Veeco) in tapping mode with an OMCL-AC160TS cantilever (Olympus). To analyze the obtained images, Nanoscope software (Veeco) was used.

RNA Stability Assay. RNA or RNP solutions were prepared as in the EMSA experiment but on a 10 μL scale. These solutions were incubated with 20% FBS (Cell Culture Bioscience) at 37 °C for 0, 0.5, 1, 2, 4, 8, 16, and 24 h. The reaction was stopped by adding 190 μL of stop solution (10 mM EDTA, 0.5% SDS). To remove the proteins, the sample was extracted with TE-saturated phenol and chloroform. After the ethanol precipitation, recovered RNAs were loaded into 5% polyacrylamide gel. Electrophoresis was conducted with 0.5× TBE at room temperature. The gel was stained with SYBR Green and observed by FLA-7000. The densities of residual RNA bands were quantified using Multi-Gauge software (Fuji-film). The values were normalized to the value at time 0. The experiments were repeated six times for 0−2 h and three times for 4−24 h, and the average values were obtained.

Conflict of Interest: The authors declare no competing financial interest.

Supporting Information Available: Supplementary experimental methods, Figures S1−S9, and Table S1. The Supporting Information is available free of charge on the ACS Publications website at DOI: 10.1021/nn5069622.

Acknowledgment. We thank Dr. Wolfgang Piendl (Innsbruck Medical University) for providing the RPL1 plasmid. We also thank Dr. Hirohide Saito (Kyoto University) and Mr. Tomoya Yamazaki (Kyoto University) for helpful suggestions and experimental information at the early stage of this research, and Mr. Fumihiko Sagawa (Kyoto University) for reading this manuscript. This work was supported by the grants from Japan Society for the Promotion of Science (numbers 23221011 and 23119005).

REFERENCES AND NOTES

1. Li, H.; Labean, T. H.; Leong, K. W. Nucleic Acid-Based Nanoengineering: Novel Structures for Biomedical Applications. *Interface Focus* **2011**, *1*, 702–724.
2. Krishnan, Y.; Simmel, F. C. Nucleic Acid Based Molecular Devices. *Angew. Chem., Int. Ed.* **2011**, *50*, 3124–3156.
3. Grabow, W.; Jaeger, L. RNA Modularity for Synthetic Biology. *F1000Prime Rep.* **2013**, *5*, 46.
4. Chworos, A.; Severcan, I.; Koyfman, A. Y.; Weinkam, P.; Oroudjev, E.; Hansma, H. G.; Jaeger, L. Building Programmable Jigsaw Puzzles with RNA. *Science* **2004**, *306*, 2068–2072.
5. Severcan, I.; Geary, C.; Verzemnieks, E.; Chworos, A.; Jaeger, L. Square-Shaped RNA Particles from Different RNA Folds. *Nano Lett.* **2009**, *9*, 1270–1277.
6. Severcan, I.; Geary, C.; Chworos, A.; Voss, N.; Jacovetty, E.; Jaeger, L. A Polyhedron Made of tRNAs. *Nat. Chem.* **2010**, *2*, 772–779.
7. Shu, D.; Shu, Y.; Haque, F.; Abdelmawla, S.; Guo, P. Thermodynamically Stable RNA Three-Way Junction for Constructing Multifunctional Nanoparticles for Delivery of Therapeutics. *Nat. Nanotechnol.* **2011**, *6*, 658–667.
8. Dibrov, S. M.; McLean, J.; Parsons, J.; Hermann, T. Self-Assembling RNA Square. *Proc. Natl. Acad. Sci. U.S.A.* **2011**, *108*, 6405–6408.
9. Grabow, W. W.; Zakrevsky, P.; Afonin, K. A.; Chworos, A.; Shapiro, B. A.; Jaeger, L. Self-Assembling RNA Nanorings Based on RNAI/II Inverse Kissing Complexes. *Nano Lett.* **2011**, *11*, 878–887.
10. Hao, C.; Li, X.; Tian, C.; Jiang, W.; Wang, G.; Mao, C. Construction of RNA Nanocages by Re-engineering the Packaging RNA of Phi29 Bacteriophage. *Nat. Commun.* **2014**, *5*, 3890.
11. Khisamutdinov, E. F.; Jasinski, D. L.; Guo, P. RNA as a Boiling-Resistant Anionic Polymer Material To Build Robust Structures with Defined Shape and Stoichiometry. *ACS Nano* **2014**, *8*, 4771–4781.
12. Jasinski, D. L.; Khisamutdinov, E. F.; Lyubchenko, Y. L.; Guo, P. Physicochemically Tunable Polyfunctionalized RNA Square Architecture with Fluorogenic and Ribozymatic Properties. *ACS Nano* **2014**, *8*, 7620–7629.
13. Khisamutdinov, E. F.; Li, H.; Jasinski, D. L.; Chen, J.; Fu, J.; Guo, P. Enhancing Immunomodulation on Innate Immunity by Shape Transition Among RNA Triangle, Square and Pentagon Nanovehicles. *Nucleic Acids Res.* **2014**, *42*, 9996–10004.
14. Guo, P. The Emerging Field of RNA Nanotechnology. *Nat. Nanotechnol.* **2010**, *5*, 833–842.
15. Guo, P.; Haque, F.; Hallahan, B.; Reif, R.; Li, H. Uniqueness, Advantages, Challenges, Solutions, and Perspectives in

Therapeutics Applying RNA Nanotechnology. *Nucleic Acid Ther.* **2012**, *22*, 226–245.
16. Ohno, H.; Kobayashi, T.; Kabata, R.; Endo, K.; Iwasa, T.; Yoshimura, S. H.; Takeyasu, K.; Inoue, T.; Saito, H. Synthetic RNA–Protein Complex Shaped Like an Equilateral Triangle. *Nat. Nanotechnol.* **2011**, *6*, 116–120.
17. Osada, E.; Suzuki, Y.; Hidaka, K.; Ohno, H.; Sugiyama, H.; Endo, M.; Saito, H. Engineering RNA–Protein Complexes with Different Shapes for Imaging and Therapeutic Applications. *ACS Nano* **2014**, *8*, 8130–8140.
18. Fujita, Y.; Furushima, R.; Ohno, H.; Sagawa, F.; Inoue, T. Cell-Surface Receptor Control That Depends on the Size of a Synthetic Equilateral-Triangular RNA–Protein Complex. *Sci. Rep.* **2014**, *4*, 6422.
19. Fei, J.; Bronson, J. E.; Hofman, J. M.; Srinivas, R. L.; Wiggins, C. H.; Gonzalez, R. L., Jr. Allosteric Collaboration between Elongation Factor G and the Ribosomal L1 Stalk Directs tRNA Movements During Translation. *Proc. Natl. Acad. Sci. U.S.A.* **2009**, *106*, 15702–15707.
20. Trabuco, L. G.; Schreiner, E.; Eargle, J.; Cornish, P.; Ha, T.; Luthey-Schulten, Z.; Schulten, K. The Role of L1 Stalk–tRNA Interaction in the Ribosome Elongation Cycle. *J. Mol. Biol.* **2010**, *402*, 741–760.
21. Hanner, M.; Mayer, C.; Kohrer, C.; Golderer, G.; Grobner, P.; Piendl, W. Autogenous Translational Regulation of the Ribosomal MvaL1 Operon in the Archaebacterium *Methanococcus vannielii*. *J. Bacteriol.* **1994**, *176*, 409–418.
22. Mayer, C.; Kohrer, C.; Grobner, P.; Piendl, W. MvaL1 Autoregulates the Synthesis of the Three Ribosomal Proteins Encoded on the MvaL1 Operon of the Archaeon *Methanococcus vannielii* by Inhibiting Its Own Translation Before or at the Formation of the First Peptide Bond. *Mol. Microbiol.* **1998**, *27*, 455–468.
23. Kraft, A.; Lutz, C.; Lingenhel, A.; Grobner, P.; Piendl, W. Control of Ribosomal Protein L1 Synthesis in Mesophilic and Thermophilic Archaea. *Genetics* **1999**, *152*, 1363–1372.
24. Nikulin, A.; Eliseikina, I.; Tishchenko, S.; Nevskaya, N.; Davydova, N.; Platonova, O.; Piendl, W.; Selmer, M.; Liljas, A.; Drygin, D.; et al. Structure of the L1 Protuberance in the Ribosome. *Nat. Struct. Biol.* **2003**, *10*, 104–108.
25. Nevskaya, N.; Tishchenko, S.; Gabdoulkhakov, A.; Nikonova, E.; Nikonov, O.; Nikulin, A.; Platonova, O.; Garber, M.; Nikonov, S.; Piendl, W. Ribosomal Protein L1 Recognizes the Same Specific Structural Motif in Its Target Sites on the Autoregulatory mRNA and 23S rRNA. *Nucleic Acids Res.* **2005**, *33*, 478–485.
26. Kohrer, C.; Mayer, C.; Neumair, O.; Grobner, P.; Piendl, W. Interaction of Ribosomal L1 Proteins from Mesophilic and Thermophilic Archaea and Bacteria with Specific L1-Binding Sites on 23S rRNA and mRNA. *Eur. J. Biochem.* **1998**, *256*, 97–105.
27. Baugh, C.; Grate, D.; Wilson, C. 2.8 Å Crystal Structure of the Malachite Green Aptamer. *J. Mol. Biol.* **2000**, *301*, 117–128.
28. Afonin, K. A.; Bindewald, E.; Yaghoubian, A. J.; Voss, N.; Jacovetty, E.; Shapiro, B. A.; Jaeger, L. *In Vitro* Assembly of Cubic RNA-Based Scaffolds Designed *in Silico*. *Nat. Nanotechnol.* **2010**, *5*, 676–682.
29. Afonin, K. A.; Viard, M.; Koyfman, A. Y.; Martins, A. N.; Kasprzak, W. K.; Panigaj, M.; Desai, R.; Santhanam, A.; Grabow, W. W.; Jaeger, L.; et al. Multifunctional RNA Nanoparticles. *Nano Lett.* **2014**, *14*, 5662–5671.
30. Geary, C.; Rothemund, P. W.; Andersen, E. S. RNA Nanostructures. A Single-Stranded Architecture for Cotranscriptional Folding of RNA Nanostructures. *Science* **2014**, *345*, 799–804.
31. Delebecque, C. J.; Lindner, A. B.; Silver, P. A.; Aldaye, F. A. Organization of Intracellular Reactions with Rationally Designed RNA Assemblies. *Science* **2011**, *333*, 470–474.
32. Sachdeva, G.; Garg, A.; Godding, D.; Way, J. C.; Silver, P. A. *In Vivo* Co-localization of Enzymes on RNA Scaffolds Increases Metabolic Production in a Geometrically Dependent Manner. *Nucleic Acids Res.* **2014**, *42*, 9493–9503.
33. King, N. P.; Sheffler, W.; Sawaya, M. R.; Vollmar, B. S.; Sumida, J. P.; Andre, I.; Gonen, T.; Yeates, T. O.; Baker, D. Computational Design of Self-Assembling Protein Nanomaterials with Atomic Level Accuracy. *Science* **2012**, *336*, 1171–1174.
34. Gradisar, H.; Bozic, S.; Doles, T.; Vengust, D.; Hafner-Bratkovic, I.; Mertelj, A.; Webb, B.; Sali, A.; Klavzar, S.; Jerala, R. Design of a Single-Chain Polypeptide Tetrahedron Assembled from Coiled-Coil Segments. *Nat. Chem. Biol.* **2013**, *9*, 362–366.
35. Fletcher, J. M.; Harniman, R. L.; Barnes, F. R.; Boyle, A. L.; Collins, A.; Mantell, J.; Sharp, T. H.; Antognozzi, M.; Booth, P. J.; Linden, N.; et al. Self-Assembling Cages from Coiled-Coil Peptide Modules. *Science* **2013**, *340*, 595–599.
36. Saito, H.; Inoue, T. Synthetic Biology with RNA Motifs. *Int. J. Biochem. Cell Biol.* **2009**, *41*, 398–404.